Observation of the flux-antiflux boundary propagation during magnetization reversal in $Bi_2Sr_2CaCu_2O_{8+\delta}$ with single vortex resolution

A. Schwarz,[a] U. H. Pi, M. Liebmann,[b] and R. Wiesendanger
Institute of Applied Physics and Microstructure Research Center, University of Hamburg, Jungiusstrasse 11, 20355 Hamburg, Germany

Z. G. Khim
School of Physics, Seoul National University, Seoul 151-742, South Korea

D. H. Kim
Department of Physics, Yeungnam University, Kyungsan 712-749, South Korea

(Received 21 June 2005; accepted 2 December 2005; published online 5 January 2006)

Snapshots of the flux distribution during magnetization reversal of a high-temperature superconductor $Bi_2Sr_2CaCu_2O_{8+\delta}$ single crystal in the presence of artificial columnar defects were recorded using magnetic force microscopy. Thereby, the flux-antiflux boundary width and its displacement by annihilation of individual vortex-antivortex pairs could be visualized. In general the flux density follows Bean's model. However, step dislocations with a strongly anisotropic pinning behavior lead locally to a nonmonotonous flux distribution and result in a delay of the boundary propagation. © *2006 American Institute of Physics*. [DOI: 10.1063/1.2161815]

During magnetization reversal of type II superconductors, regions occupied by vortices of opposite polarity are separated by a flux-antiflux boundary. Flux penetration into the specimen and the general features of the reversal process are described by the longitudinal[1] and transversal[2] Bean model, respectively. Its basic statement is that the current density $\mathbf{J}=\nabla\times\mathbf{H}_a$, which is induced at the surface to exclude the externally applied magnetic field $\mathbf{H}_a$, exerts a certain Lorentz force density $\bar{\mathbf{F}}_L=\mathbf{J}\times\bar{\mathbf{B}}$ on the penetrating local average magnetic flux density $\bar{\mathbf{B}}$. Thereby, the flux is displaced from the sample edges towards the center, whenever the critical current density J_c is reached and $\bar{\mathbf{F}}_L$ exceeds the mean pinning force density $\bar{\mathbf{F}}_{\mathrm{pin}}$, which originates from sample imperfections. If the field magnitude is reduced, vortices leave the sample starting from the edges. If the field direction is reversed, vortices of opposite polarity (*antivortices*) penetrate from the edges, whereby a flux-antiflux boundary is introduced into the sample. Note that the Bean model neglects flux quantization, averages over distances much larger than the intervortex spacing, and does not discriminate between different types of defects. Therefore, this model does not make any statements about the fine structure of the boundary region, where vortices and antivortices coexist, and the influence of different types of defects.

An understanding of the magnetization process and the influence of pinning is mandatory to develop devices based on superconducting materials. Naturally, high-temperature superconductors are of particular interest. Up to now, magneto-optical means have been employed to investigate flux distributions with respect to the Bean model in such materials (see, e.g., Jooss[3] for a review), but the resolution is diffraction limited. On the other hand, magnetic force microscopy (MFM) has proven its capability to detect individual vortices via their magnetic field in the low flux density regime.[4] If the magnetic fields of neighboring vortices strongly overlap (high flux density regime), flux density variations can still be imaged, because the MFM signal is proportional to the magnetic field generated by the total flux.[5] Moreover, this technique allows to image the surface topography with high resolution, e.g., monoatomic step heights are easily resolved, whereby structural defects can be examined with respect to their pinning properties.[5,6] Here we present a MFM study of the flux-antiflux boundary propagation during magnetization reversal of a $Bi_2Sr_2CaCu_2O_{8+\delta}$ single crystal platelet. Since single vortex resolution is obtained, information beyond the Bean model becomes directly accessible.

All experiments have been performed with our home built force microscope (*Hamburg design*),[7] which is operated in ultrahigh vacuum, at a base temperature of 5.2 K and in an externally applied magnetic field up to $\mu_0 H_a = B_a = 5$ T. A cantilever with a ferromagnetic iron coated tip at its free end is utilized to detect the tip-sample interaction via the frequency modulation technique. Surface topography as well as magnetic properties can be probed with appropriate data acquisition schemes. To record MFM images we chose a scan height h of about 18 nm and a cantilever oscillation amplitude $A=10$ nm. Details of the experimental setup, procedures, modes of operation can be found in Ref. 7.

The $Bi_2Sr_2CaCu_2O_{8+\delta}$ single crystal (about $a\times b\times c = 2.2\ \mathrm{mm}\times 0.72\ \mathrm{mm}\times 0.048\ \mathrm{mm}$ in size) was grown by a floating zone method and then irradiated with 1.3 GeV uranium ions to form artificial columnar defects[8] parallel to the c axis. They act as strong pinning centers.[5] The ion dose corresponded to a matching flux density of $B_m=2$ mT. Furthermore, stacking fault dislocations, which exhibit an anisotropic pinning behavior,[9] are present in the investigated crystal.

Tip axis, crystal c axis and magnetic field direction are oriented normal to the sample surface (z direction). After magnetizing the tip in $B_a=+100$ mT parallel to the tip axis, the sample was field cooled from above T_c down to T

[a]Author to whom correspondence should be addressed; electronic mail: aschwarz@physnet.uni-hamburg.de
[b]Present address: II. Department of Physics, RWTH Aachen, 52056 Aachen, Germany.

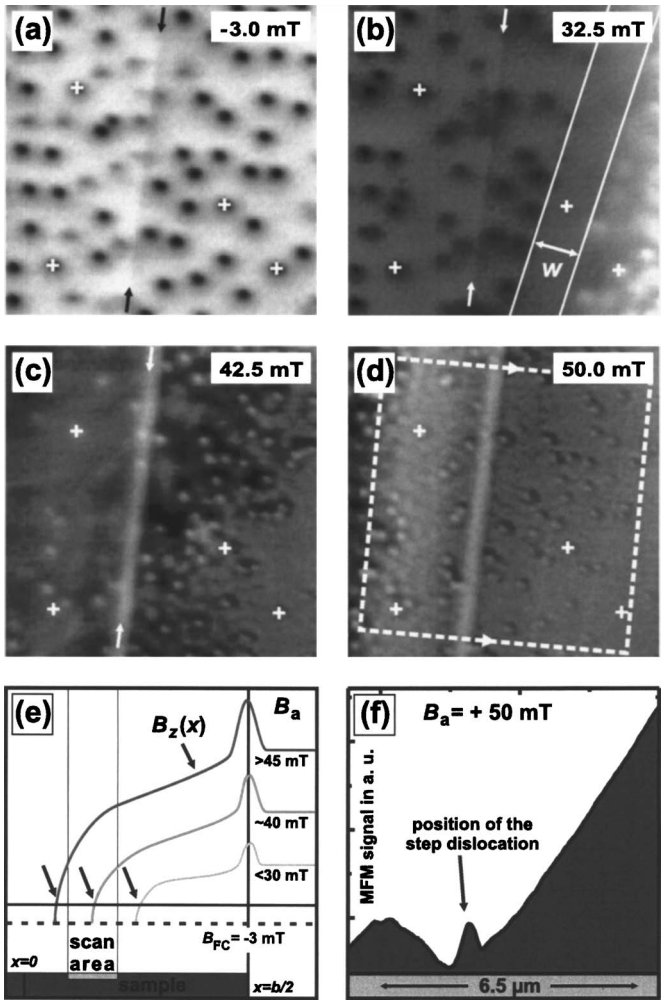

FIG. 1. (a) MFM image of the flux glass state after field cooling in $B_{FC}=-3$ mT (scan area: $a_{scan}=7\ \mu m\times 7\ \mu m$). (b) After increasing B_a to 32.5 mT, the flux-antiflux boundary is visible as *zone of zero vortex density* between the parallel lines separated by $w\approx 1\ \mu m$. (c) At 42.5 mT the antivortices have reached the line defect (marked by arrows), which now appears as bright strip. (d) The situation after complete magnetization reversal of the scan area. (e) Sketch of the experimental situation according to the one-dimensional transversal Bean model.[2] Flux penetration $B_z(x)$ (mirror symmetric with respect to the sample center at $x=0$) with increasing field and propagation of the boundary (see arrows) with respect to the scan area is shown. The dashed line corresponds to the homogeneous flux density after field cooling. (f) Averaged cross section taken perpendicular to the line defect in the boxed area from (d). Due to the stacking fault dislocations, the flux density does not change monotonically.

$=5.2$ K in $B_a=B_{FC}=-3$ mT. Then, B_a was ramped stepwise from −3 to +50 mT. To study the magnetization reversal and in particular the mechanisms of the boundary displacement, snapshots of the vortex configuration were recorded for each B_a on the same sample area. Four of them are displayed in Figure 1(a)–1(d). For comparison, the flux density $B_z(x)$ and its evolution with increasing B_a according to the one-dimensional Bean model is sketched in (e).

The glass-like random vortex configuration after field cooling is imaged in (a). Since MFM detects the magnetic field associated with the quantum flux $\Phi_0=2\cdot 10^{-15}$ T m^{-2}, each vortex appears as a dot with a radius on the order of the London penetration depth λ (for $Bi_2Sr_2CaCu_2O_8$ $\lambda\approx 200$ nm). The dark contrast indicates a repulsive tip-vortex interaction, i.e., tip magnetization and vortex polarity are antiparallel. The total number of $N=B_{FC}\cdot a_{scan}/\Phi_0=62$ vortices corresponds reasonably well to $B_{FC}=-3$ mT and the scan area $a_{scan}=49\ \mu m^2$. Four strong pinning sites are marked by crosses, to evalute their role during magnetization reversal. For the same reason, the barely visible faint line is marked by two arrows. At the corresponding position in the topography image a step with a height of about (0.36 ± 0.05) nm was found at exactly that position. Previously, we identified such straight steps with heights less than the surface cleavage step height of $c/2=1.55$ nm as stacking fault dislocations and reported a strongly anisotropic pinning behavior.[9] After applying a field opposite to the direction during field cooling, antivortices enter the sample from the edges, where the magnetization reversal due to individual vortex-antivortex annihilation processes starts. At 30 mT the first antivortices enter the scan area. In (b) the situation at 32.5 mT is shown. The incoming antivortices (bright contrast due to the attractive tip-vortex interaction) already penetrated the scan area from the right. The four crosses mark the same strong pinning sites as identified in (a). While the two on the left are still occupied by vortices, the one between the two parallel white lines is empty and the right one is already occupied by an antivortex. Vortices and antivortices are well separated from each other by an about 1-μm-wide *zone of zero vortex density* marked by two parallel white lines, where neither vortices nor antivortices are detected. The following propagation mechanism can be inferred: In the boundary region flux closure is achieved by the formation of vortex-antivortex loops. Since the antivortices are driven towards the sample center by the Lorentz force, their radii shrink with increasing B_a. Finally, the loop collapses below a certain radius, if its elastic energy becomes larger than its pinning energy. Thereby, a vortex-antivortex pair is annihilated. The remaining empty columnar defect is reoccupied by another mobile incoming antivortex. Note that the loop is rather asymmetric, since only the mobile antivortex part moves towards the rather fixed strongly pinned vortex part.

The width w of the zone of zero vortex density is related to the range of the attractive vortex-antivortex force $F_{V\text{-}AV}$ and the pinning force. The attraction between vortices of opposite polarity can be approximated using $F_{V\text{-}AV}=-L\cdot\Phi_0^2/(4\pi\mu_0\lambda^2)\cdot K_0'(r/\lambda)$. Here, r is the vortex-antivortex separation, L is the length of the vortex line, and $K_0'(r/\lambda)$ is the derivative of the modified Bessel function, which has the form $K_0(r/\lambda)=(\pi\lambda/2r)^{1/2}\cdot e^{-r/\lambda}$ for $r\gg\lambda$.[10] Since $F_{V\text{-}AV}$ decays exponentially, the characteristic decay length λ, w is expected to be not much larger than a few λ, which agrees well with our observation of $w\approx 5\lambda$. Using $r=w$ and $L=c$, i.e, the platelet thickness, an attractive force of 7 pN can be estimated, which should correspond approximately to the pinning strength of the mobile incomming vortices. Note further that since the typical lateral dragging force exerted by the scanning tip on a vortex is only about 1.5 pN in our experimental situation,[11] the influence of the measurement procedure on the genuine vortex arrangement is negligible.

In (c) the antivortex front has reached the stacking fault dislocation (see arrows). It now appears as a bright strip. In a previous investigation[9] we found vortices are quite mobile along such line defects, while they are strongly trapped in the perpendicular direction. For an attractive tip-vortex interaction, vortices are attracted towards the tip if scanned across the line defect, whereby the whole dislocation step appears bright, even if only a few vortices are attached to the line defect. If the tip-vortex interaction is repulsive, as in (a) and

(b), vortices are pushed to the side along the line defect and are therefore not imaged. Note further, that on the left side of the line defect only a few individual antivortices are visible, while their density is much larger on the right side. This inhomogeneous distribution occurs because the line defect can accommodate a large amount of vortices, which then repel vortices of the same polarity. Clearly, the advance of the flux-antiflux boundary is severely hindered by the presence of a continuous line defect perpendicular to the propagation direction than by a porous random distribution of point-like defects.

Further increasing of B_a results in a complete magnetization reversal of the imaged area, as visible in (d). The vortex density is so large that only the strongly pinned vortices can be identified, because they repel the more mobile vortices, leaving a dark ring around them. According to the transversal Bean model sketched in (e), the vortex density between the flux-antiflux boundary and the sample edges should decrease monotonically towards the sample center. Since the magnitude of the MFM signal is proportional to the magnetic field generated by the vortices, flux density variations can still be detected.[5] In (f) the average cross section taken perpendicular to the incoming vortex front from the boxed area in (d) is displayed. Right to the line defect a steady decrease of the vortex density towards the sample center is observed. On the line defect itsself the density is enhanced, but reduced in the vicinity, due to the repulsion between vortices of the same polarity. Thereby, a nonmonotonic flux distribution is induced near the stacking fault dislocations. It can be concluded that randomly distributed point defects result in a vortex distribution as predicted by the Bean model, while strong deviations are induced by extended line defects, which can accomodate a large number of vortices.

In summary, we demonstrated that MFM is a suitable technique to visualize the dynamics of the magnetization reversal and particularly the propagation of the flux-antiflux boundary in type II superconductors with single vortex resolution. In our case the boundary consists of a 5λ wide zone of zero vortex density, which propagates by annihilation of vortex-antivortex pairs. Line defects with a strong pinning effect delay a transversal movement of the boundary and cause a nonmonotonic flux distribution in their vicinity after complete magnetization reversal. In regions with columnar defects the resulting flux density decreases monotonously towards the sample center, as predicted by the Bean model.

Financial support from the DFG and from the NSI (NCRC) program of KOSEF, Korea, is gratefully acknowledged.

[1] C. P. Bean, Phys. Rev. Lett. **8**, 250 (1962).
[2] E. H. Brandt and M. Indenbom, Phys. Rev. B **48**, 12893 (1993); E. Zeldov, J. R. Clem, M. McElfresh, and M. Darwin, Phys. Rev. B **49**, 9802 (1994).
[3] C. Jooss, Rep. Prog. Phys. **65**, 651 (2002).
[4] See, e.g., A. Moser, H. J. Hug, I. Parashikov, B. Stiefel, O. Fritz, H. Thomas, A. Baratoff, H. J. Güntherodt, and P. Chaudhari, Phys. Rev. Lett. **74**, 1847 (1995); A. Volodin, K. Temst, C. Van Haesendonck, and Y. Bruynseraede, Appl. Phys. Lett. **73**, 1134 (1998); M. Roseman and P. Grütter, New J. Phys. **3**, 24 (2001).
[5] U. H. Pi, Z. G. Khim, D. H. Kim, U. Kaiser, A. Schwarz, M. Liebmann, and R. Wiesendanger, J. Low Temp. Phys. **131**, 993 (2003).
[6] A. Moser, H. J. Hug, B. Stiefel, and H. J. Güntherodt, J. Magn. Magn. Mater. **190**, 114 (1998).
[7] M. Liebmann, A. Schwarz, S. M. Langkat, and R. Wiesendanger, Rev. Sci. Instrum. **73**, 3508 (2002).
[8] T. W. Lee, C. W. Lee, S. Y. Shim, D. H. Ha, and D. H. Kim, Prog. Supercond. **3**, 36 (2001).
[9] U. H. Pi, Z. G. Khim, D. H. Kim, A. Schwarz, M. Liebmann, and R. Wiesendanger, Phys. Rev. B **69**, 094518 (2004).
[10] E. H. Brandt, Physica C **369**, 10 (2002).
[11] U. H. Pi, Z. G. Khim, D. H. Kim, A. Schwarz, M. Liebmann, and R. Wiesendanger, Appl. Phys. Lett. **85**, 5307 (2004).